EE 230C: SOLID STATE ELECTRONICS
FINAL PROJECT
20 DECEMBER 2024

Elizabeth Juette, Vir Karan, Wayne Zhao

INTRODUCTION

This project involves modeling the monolayer MoS_2 transistor in Ref. [1] using the quasi-ballistic MOSFET models discussed in class. The bandstructure calculations necessary for deriving the I-V characteristics use the Slater-Koster parameters provided in Ref. [2]. Following these calculations, we provide a brief discussion on the model performance compared to experimental data, and we assess the efficacy of the transistors based on these materials for future electronics.

1. CURRENT-VOLTAGE CHARACTERISTICS

Using the quasi-ballistic MOSFET models discussed in the class, we analyze the current voltage characteristics of the MoS_2 device. The following sections will discuss the bandstructure calculations, estimation of series resistances, and analysis of the IV curve.

1.1 Bandstructure

Figure 1 illustrates the MoS_2 geometry: the nearest-neighbors for Mo-Mo and S-S bonds have an interatomic distance of a = 3.16Å, with the interatomic distance between Mo-S being b = 2.41Å. The primitive cell for MoS_2 contains one Mo and 2 S atoms (one above and one below the Mo plane). Assuming a perfect rhombohedral lattice, the primitive lattice vectors are:

$$R_1 = a\,(1,0,0)$$
$$R_2 = a\left(\frac{1}{2}, \frac{\sqrt{3}}{2}, 0\right)$$

The reciprocal lattice vectors are then:

$$K_1 = \frac{4\pi}{\sqrt{3}a}\left(\frac{\sqrt{3}}{2}, -\frac{1}{2}, 0\right)$$
$$K_2 = \frac{4\pi}{\sqrt{3}a}\,(0,1,0)$$

The high symmetry points in the first Brillouin zone are:

$$\Gamma = (0,0)$$
$$K = \left(\frac{2\pi}{3a}, -\frac{2\pi}{\sqrt{3}a}\right)$$
$$M = \left(\frac{\pi}{a}, -\frac{\pi}{\sqrt{3}a}\right).$$

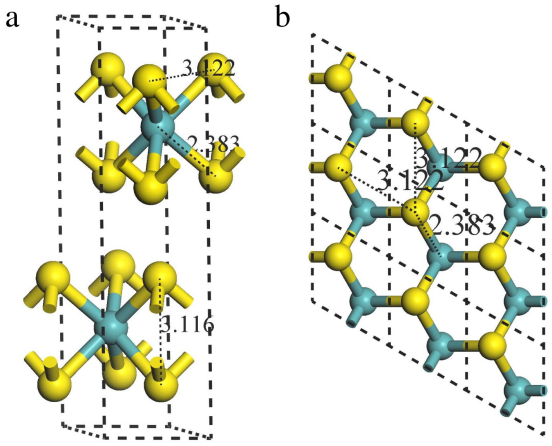

FIGURE 1: Geometry of MoS_2 where (a) is a side view of a bulk unit cell with Sulfur atoms represented by yellow and Molybdenum atoms by blue. (b) Top view of a MoS_2 monolayer. Figure courtesy of Ref. [3].

The tight-binding Hamiltonian of one unit cell interacts with the states from 6 neighboring cells, and this interaction can be broken down and written purely as overlap between the atomic basis states present in each unit cell (ϕ_j). For example, for a state ϕ_j^n of unit cell n present at a distance $\vec{d}$ away from state ϕ_i^n of unit cell n, we can write the overlap as:

$$E_{\phi_i,\phi_j}(\vec{d}) = < \phi_i^n(\vec{r})|H|\phi_j^n(\vec{r}+\vec{d}) > = \int dr^3 \phi_i^{*n}(\vec{r})\hat{H}\phi_j^n(\vec{r}+\vec{d})$$

The overlap integral above can be written as a function of the Slater-Koster tight binding parameters and the direction cosines (l,m,n) connecting the two states using Table I of [4]. Correspondingly, the overlap of state ϕ_i^n of cell n with ϕ_j^m of cell m can be written as:

$$H_{\phi_i,\phi_j}(\vec{d}) = E_{\phi_i,\phi_j} e^{i\vec{k}\cdot\vec{d}}$$

In general, the $(i,j)^{th}$ element (corresponding to the overlap of the ϕ_i and ϕ_j basis states) of the tight-binding Hamiltonian is:

$$H_{ij} = \Sigma_{\vec{d}} E_{\phi_i,\phi_j} e^{i\vec{k}\cdot\vec{d}}$$

Here, the summation is over all pairs of states that are nearest-neighbors, separated by vector $\vec{d}$. For MoS_2, each Mo atom has 6 S neighbors separated by the vectors $\{\frac{a}{2} < 1, \frac{\sqrt{3}}{3}, \pm 1 >, \frac{a}{2} <$

$-1, -\frac{\sqrt{3}}{3}, \pm 1 >, \frac{a}{2} < 0, \frac{2\sqrt{3}}{3}, \pm 1 >\}$. There are also Mo-Mo nearest neighbors (technically next-nearest neighbors) and S-S neighbors (in-plane) separated by $\{\pm\frac{a}{2} < 2, 0, 0 >, \pm\frac{a}{2} < 1, \sqrt{3}, 0 >, \pm\frac{a}{2} < -1, \sqrt{3}, 0 >\}$. We also have to consider interactions between the S atoms within the same cell, which are separated by $\{\frac{a}{2} < 0, 0, 2 >\}$. We can then write out the Hamiltonian after considering the overlaps for the above sets of separation vectors ($\mathbf{h} = [H_{ij}]$), and find the eigenvalues to get the bandstructure of MoS_2 monolayers.

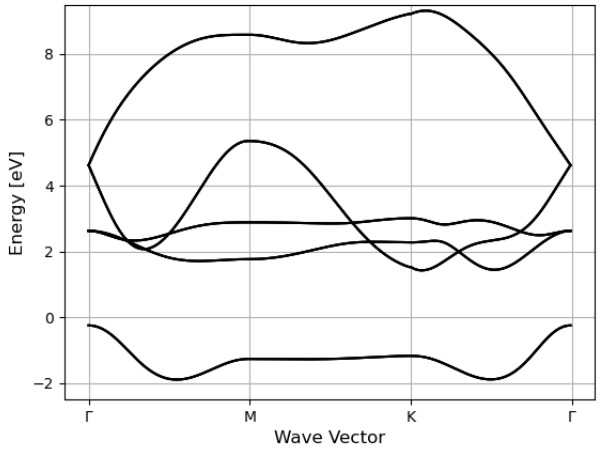

FIGURE 2: Bandstructure for monolayer MoS_2 obtained through the tight-binding approach, plotted along the $\Gamma - M - K - \Gamma$ direction. As can be seen, this structure shows a direct bandgap around the K point.

We considered two different basis sets for the problem: 1. the set of d^5 orbitals from Mo and the p^3 orbitals from the two S, giving 11 states (`TB11`); 2. the full set of sp^3d^5 orbitals from Mo and the two S giving 27 states (`TB27`). The first is easier to solve, for which we followed the simplifications done by [5] and [6] based on symmetry. For the second basis set, we approach the problem fully numerically, and used the Slater-Koster parameters as computed in [2]. Code for both approaches can be found at `https://github.com/vir-k01/EE230C`. This case is essentially a generalization of the basis set from the first case. The bandstructure plotted for either case is very similar around the bandgap (energy between -2 and +7 eV), which is shown in Figure 2. This bandstructure, although not identical to previous works in the literature [2, 5], recovers the features needed to compute transport correctly: there is a direct bandgap around the K point, and an indirect gap originating close to the Γ point. Although we overestimate the direct gap here, we expect the transport properties (which depend on the curvature of the conduction band) to be very similar to those found in the literature.

1.2 Quasi-Ballistic Model

The current-voltage performance curve is calculated using the quasi-ballistic MOSFET model we learned in class. The procedure requires self-consistent calculations of the ψ_s potential. The main equation used in our algorithm is from the EE230C Reader Eq. (5.37) which is presented as Eq. (1) in this report:

$$I = WC\,(V_G - V_{REF})\,v_T \frac{1 - r_s}{1 + r_s} \frac{1 - \frac{1-r_D}{1-r_s} e^{-\frac{eV_{DS}}{k_B T}}}{\frac{1}{1+r_s} + \frac{1-r_D}{1+r_s} e^{-\frac{eV_{DS}}{k_B T}}} \tag{1}$$

where the electron density n_s is given by Eq. (2):

$$n_s = \left(\frac{m^* k_B T}{2\pi\hbar^2}\right) e^{\eta_s} \left[1 + (1 - r_D) e^{-\frac{eV_{DS}}{k_B T}}\right] \tag{2}$$

$$= C\,(V_G - V_{REF}) \tag{3}$$

We also know the following definitions from our in-class derivation of the quasi-ballistic model:

$$\eta_s = \frac{\mu_S - E_C}{k_B T}$$

$$v_T = \sqrt{\frac{2k_B T}{\pi m^*}}$$

$$Q = e \int f_0 D(E - U) dE$$

To complete the self-consistent model in our algorithm, we also use Eq. (1.2) while also acknowledging the Q presented in the class Reader notes as Eq. (1.40). We also acknowledge that $E_{C(\text{tob})}$ is related to Eq. (1.2) through the definition of η_s. The surface potential in the channel is given by Eq. (1.2).

$$dU = \frac{C_G}{\sum C}(-eV_G) + \frac{C_D}{\sum C}(-eV_D) - \frac{edQ}{\sum C} \tag{3}$$

$$\psi_S(\text{when off}) = \alpha_G V_G + \alpha_D V_D \tag{3}$$

To complete our model, we allowed the reflection probabilities and capacitance variables to float as fitting parameters. The results are back-inferred values of these parameters from the experimental data and a quasi-ballistic model with a reasonable fit to the data.

We can find an approximate value for α_G and α_D using the subthreshold slope (SS) and DIBL provided by the data and Eq. (1.2) and Eq. (1.2).

$$SS = \frac{2.3 k_B T}{\alpha_G} \tag{3}$$

$$DIBL = \frac{V_T^l - V_T^h}{V_D^h - V_D^l} = \frac{\alpha_D}{\alpha_G} - \frac{1}{\alpha_G} \frac{\psi_S^h - \psi_s^l}{V_D^h - V_D^l} \tag{3}$$

The provided paper and data shows $SS < 93mV/dec$ and $DIBL < 0.425V/V$. We also know from the derivation in class and Eq. (5.57) in the Reader notes that:

$$\psi_l^h - \psi_s^l = \frac{k_B T}{e} \ln \frac{V_D^l}{k_B T/e}$$

We combined the known parameters derived from the data and the equations indicated above to determine α_G, α_D, and integrated the results in our self-consistent algorithm for determining the IV characteristics.

The current voltage characteristics determined using our code is presented in Fig. 3. While it is clear that our plot is not a

perfect fit to the data for this case with $V_G = 0$, that can attributed to our fitting parameters. If we persisted with further iterations in our genetic algorithm to converge on improved solutions than the m^*, α, r_s, r_D, series resistances and other physical parameters impacting the shape of our prediction, we may have been able to produce a better result. As it is, Fig. 3 shows that the subthreshold swing shown in the model, or $SS = \frac{\partial \log I}{\partial V_G}^{-1}$ is slightly off from what the data presents. This essentially means that the interpreted values we are using for C_D and C_{ox} in $SS = 60 \times (1 + C_D/C_{ox})$ from the Reader notes Eq (5.51) is not perfectly optimized to match the experimental values.

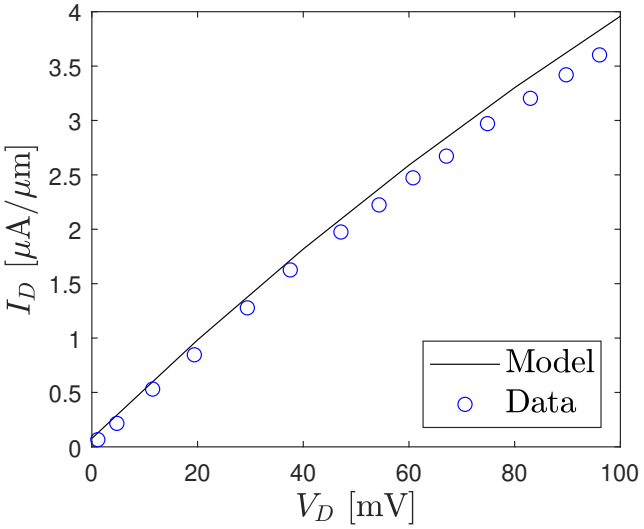

FIGURE 3: Current-Voltage characteristics of the MoS_2 transistor using the effective mass and quasi-ballistic MOSFET model with self-consistency.

For Fig. 3 and Fig. 4, we picked a few points off of the plots in Figure 5.b. and Figure 5.c. presented in the provided paper. Figure 4 also shows that our model is not a perfect fit to the data. However, for the select snapshot of given voltages at a $V_D = 0.2$ V, we have a reasonable fit to the data with some variation in the curvature of our model prediction versus the data.

Note also that we used fitting parameters to approximate the effect of series resistance on the voltages seen by the actual device. In class, we discussed that it is important to consider the difference between applied and seen voltages. Equation 1.2 presents an example of this effect:

$$V_D = V_D^A - I(R_S + R_D) \tag{3}$$

where R_S and R_D are the source and drain contact resistances, respectively, V_D^A is the applied drain voltage, and V_D is the drain voltage seen by the device. We used optimization techniques to account for this effect in our model.

The code for the basic function used to compute the I-V results presented in this section are available in Appendix A. This function was reused with varying values of the physical parameters and applied voltages to predict device performance. We then used standard MATLAB code to generate figures and iterate

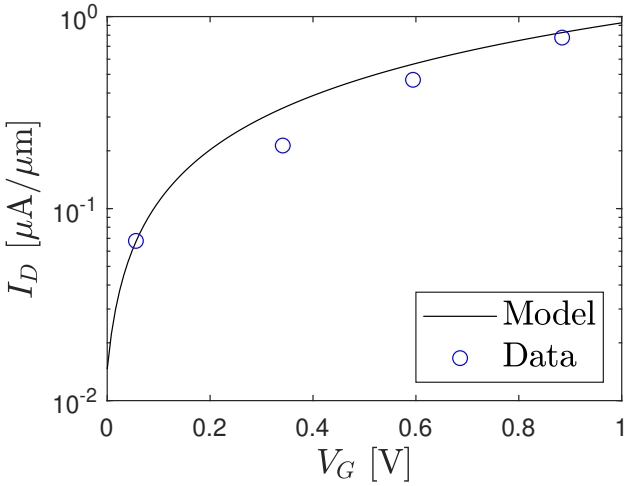

FIGURE 4: Current-Voltage characteristics of the MoS_2 transistor using the effective mass and quasi-ballistic MOSFET model with self-consistency at a V_D = 0.2 V and varying gate voltages.

through fitting parameters, re-calling the function in Appendix A for each iteration.

1.3 Contact Resistance

During the final lecture of the semester, we discussed how to determine the contact resistance for a transistor. First, we begin with Eq.(1.3):

$$I_D = \frac{W}{L}\mu^{app} C\,(V_{GS} - V_{TH})\,V_{DS} \tag{3}$$

where μ^{app} is the applied mobility, V_{GS} is the gate voltage seen by the device, V_{TH} is the threshold voltage, and V_{DS} is the drain voltage seen by the device. We then use Eq.(1.3) and Eq.(1.3) to characterize transport parameters.

$$V_{DS} = V_{DS}^A - I(R_S + R_D)$$
$$\frac{1}{\mu^{app}} = \frac{1}{\mu_B} + \frac{1}{\mu}$$

Here, V_{DS}^A is the applied drain voltage, R_S is the source contact resistance, R_D is the drain contact resistance, μ_B is the ballistic mobility, and μ is the actual mobility.

To find the series resistance, we can plot the resistance with the gate voltage and observe the vertical shift of the plot using Eq.(1.3):

$$R^{-1} = \frac{\partial I_D}{\partial V_{DS}} = \frac{W}{L} C(V_{GS} - V_{TH})\mu^{app} \tag{3}$$

This was the procedure we learned in the final lecture of the course. As shown in the figure, using the IV data provided in the paper we can find an effective series resistance near 0.4Ω.

However, for our model we found it more effective to allow this variable to float as a parameter in an optimization scheme (Genetic Algorithm). Using this approach, we had an easier time converging on a solution that also accounted for scattering in the Quasi-Ballistic transport model.

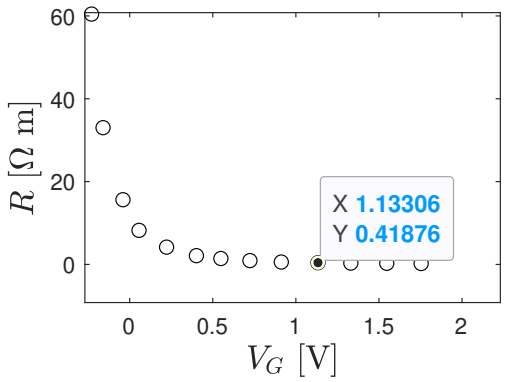

FIGURE 5: Resistance versus Gate Voltage

2. INJECTION VELOCITY AND ENERGY

The injeciton velocity, as derived from the bandstructure, is given by:

$$v_{inj} = \frac{1}{\hbar}\frac{\partial E}{\partial k} \tag{3}$$

We find $v_{inj} = 6.907 \times 10^5$m/s at the K-point in the x-direction by numerical differentiation of the conduction band. This matches quite well with previous measurements of the injection velocity[7]. On the other hand, the effective mass is defined by Eq.(2):

$$m^* = \frac{\hbar^2}{\frac{\partial^2 E}{\partial k^2}} \tag{3}$$

Using numerical differentiation, we find the effective mass at the K-point is $0.2746m_0$ in the x-direction (m_x^*) and $0.2734m_0$ in the y-direction (m_y^*), where m_0 is the mass of the free electron. Hence, the effective mass is essentially isotropic in the plane of MoS_2, which matches existing literature [2]. The injection velocity can then be obtained as:

$$v_{inj} = \sqrt{\frac{2k_BT}{\pi m_x^*}}\frac{1-\exp\frac{-qV_{DS}}{k_BT}}{1+\exp\frac{-qV_{DS}}{k_BT}}$$

Using this relation gives $v_{inj} = 1.026 \times 10^5$m/s for high V_{DS} and $T = 300K$ (i.e., the upper bound for v_{inj}), which is less than an order of magnitude different from the v_{inj} obtained from Equation 2. Hence, for this case using the effective mass to compute transport properties is a valid approximation. This is easily rationalized since the conduction band in Figure 2: a parabolic relation fits the minimum around the K-point fairly well.

3. DISCUSSION

Question: Explain how well the quasi-ballistic model explains data by using low field mobility as a fitting parameter.
Answer: Using low-field mobility as a fitting parameter is effective when the material is a conductor, such as graphene [8]. However, mobility alone cannot be used for insulators like 2D MoS_2, as a threshold voltage must be reached before the material begins to conduct, unlike graphene. This threshold voltage then becomes a secondary fitting parameter and can be variable [9]. For an insulator like MoS_2, the threshold voltage introduces a linear region in the IV curves that necessitates additional parameters to account for scattering and imperfect channel coupling. These factors lead to decreased transmission that is not accounted for in the model.

$$I = WC\,(V_G - V_{REF})\,\frac{v_{inj}^+}{1+\frac{v_T}{\mu E_{top}}} \tag{3}$$

Question: Discuss the issues involved in analyzing device data with this model.
Answer: Materials are often imperfect, with defects that decrease the coupling coefficients between the drain and the channel (source) [9]. Additionally, impurities or phonons can cause scattering, leading to a decrease in the overall transmission through the channel. Regarding the IV curves, there may be variance in the threshold voltage, as temperature can affect it, making it challenging to tune the parameters accurately.
Question: Which regions of current voltage curve may this model not work? Why?
Answer: Lee et al. demonstrate that the linear region is not well represented by the existing model due to the real material's imperfect drain-channel coupling and the lack of accounting for scattering [9]. In the linear region of the current-voltage (I-V) curve, the occupancy of the left-moving modes at the source end is underestimated, resulting in an underestimation of the linear portion of the IV curve [9, 10]. To address this, parameters such as transmission probability and drain-channel coupling are included to improve the model. The transmission probability parameter accounts for scattering in the quasi-ballistic model, while the drain-channel coupling, representing the fraction of the drain Fermi level at the source end, can be set to a value less than perfect coupling (less than 1) [9]. Lee et al. also show that the saturation region is accurately modeled using just low-field mobility [9].
Question: Include your assessment of efficacy of the transistors based on these materials for future electronics.
Answer: In assessing the efficacy of transistors based on MoS_2 for future electronics, it is evident that MoS_2 holds significant promise for scaling down MOSFETs and providing enhanced control compared to graphene. However, several engineering challenges must be addressed to realize the full potential of MoS_2 MOSFETs in future electronic applications.

A primary challenge is achieving a perfect interface between the drain and the channel, which is crucial for optimizing the coupling coefficient and transmission probabilities [9, 11]. These parameters need to be maximized to ensure the ideal current flow through the transistor.

The optimization of these transistors should strike a balance between the size and control of the MOSFETs. Monolayer MoS_2 offers the potential for minimizing the size of the device, and considerable research efforts are focused on improving control mechanisms.

As devices become smaller, they are increasingly susceptible to short channel effects, such as tunneling currents [12]. MoS_2, with its inherent band gap, is slightly better at preventing tunneling compared to graphene. The band gap in MoS_2 allows for the

creation of distinct off and on states, requiring a threshold voltage to achieve the on-state and mitigate tunneling [12].

ACKNOWLEDGMENTS

Thank you to our favorite GSI. Pratik, we are grateful for your help, patience, and explanations throughout the semester.

REFERENCES

[1] Xie, L., Liao, M., Wang, S., Yu, H., Du, L., Tang, J., Zhao, J., Zhang, J., Chen, P., Lu, X., Wang, G., Xie, G., Yang, R., Shi, D. and Zhang, G. "Graphene-Contacted Ultrashort Channel Monolayer MoS2 Transistors." *Advanced Materials* Vol. 29 No. 37 (2017): p. 1702522. DOI https://doi.org/10.1002/adma.201702522.

[2] Mishra, V., Smith, S., Liu, L., Zahid, F., Zhu, Y., Guo, H. and Salahuddin, S. "Screening in Ultrashort (5 nm) Channel MoS2 Transistors: A Full-Band Quantum Transport Study." *IEEE Transactions on Electron Devices* Vol. 62 No. 8 (2015): pp. 2457–2463. DOI 10.1109/TED.2015.2444353.

[3] Kadantsev, E. S. and Hawrylak, P. "Electronic structure of a single MoS2 monolayer." *Solid State Communications* Vol. 152 No. 10 (2012): pp. 909–913. DOI https://doi.org/10.1016/j.ssc.2012.02.005.

[4] Slater, John C and Koster, George F. "Simplified LCAO method for the periodic potential problem." *Physical review* Vol. 94 No. 6 (1954): p. 1498.

[5] Ridolfi, Emilia, Le, Duy, Rahman, TS, Mucciolo, ER and Lewenkopf, CH. "A tight-binding model for MoS2 monolayers." *Journal of Physics: Condensed Matter* Vol. 27 No. 36 (2015): p. 365501.

[6] Shahriari, Majid, Dezfuli, Abdolmohammad Ghalambor and Sabaeian, Mohammad. "Band structure and orbital character of monolayer MoS2 with eleven-band tight-binding model." *Superlattices and Microstructures* Vol. 114 (2018): pp. 169–182.

[7] English, Chris D, Smithe, Kirby KH, Xu, Runjie Lily and Pop, Eric. "Approaching ballistic transport in monolayer MoS 2 transistors with self-aligned 10 nm top gates." *2016 IEEE International Electron Devices Meeting (IEDM)*: pp. 5–6. 2016. IEEE.

[8] Lee, Ji Ung. "Quasi-ballistic transport model for nanoscale MOSFETs: learnings from a diffusive conductor." *Japanese Journal of Applied Physics* Vol. 60 No. 4 (2021): p. 044001.

[9] Lee, Ji Ung, Cuduvally, Ramya, Dhakras, Prathamesh, Nguyen, Phung and Hughes, Harold L. "Two-parameter quasi-ballistic transport model for nanoscale transistors." *Scientific Reports* Vol. 9 No. 1 (2019): p. 525.

[10] Natori, Kenji. "Ballistic metal-oxide-semiconductor field effect transistor." *Journal of applied Physics* Vol. 76 No. 8 (1994): pp. 4879–4890.

[11] Liu, Han, Neal, Adam T, Du, Yuchen and Peide, D Ye. "Fundamentals in MoS2 transistors: Dielectric, scaling and metal contacts." *ECS Transactions* Vol. 58 No. 7 (2013): p. 203.

[12] Wu, Fan, Tian, He, Shen, Yang, Hou, Zhan, Ren, Jie, Gou, Guangyang, Sun, Yabin, Yang, Yi and Ren, Tian-Ling. "Vertical MoS2 transistors with sub-1-nm gate lengths." *Nature* Vol. 603 No. 7900 (2022): pp. 259–264.

APPENDIX A. SELF-CONSISTENT ALGORITHM

```
function [Vout, J] = IVeta(U0, kT, m, rs
    , rd, W, Vg, alphaG, alphaD)
    %% Constants
    hbar = 1.055e-34; % [J s]
    q    = 1.602e-19; % [C]
    hbareV = hbar/q; % [eV]
    ns0 = m*kT/(2*pi*hbareV^2);
    vt = sqrt(2*kT/(pi*m));

    %% Energy grid
    NE = 501;
    E = linspace(-1,1,NE);
    dE = E(2)-E(1);
    D = (m/(2*pi*hbareV^2)); %
       Lorentzian Density of states per
       eV
    D = D./(dE*sum(D));  % Normalizing
       to one

    %% Bias
    IV = 500;
    VV = linspace(0,1,IV);
    for iV = 1:IV
        Vd = VV(iV);
        eta0  = -((alphaG*Vg)+(alphaD*Vd
           ))/kT;
        etas = 0;
        dU  = 1;
        while dU > 1e-6
            f = 1./(1+exp(-eta0 + etas))
               ;
            N(iV) = dE*sum(D.*f);
            etaNew = U0*N(iV);
            dU=abs(etas-etaNew);
            etas = etas+0.0001*(etaNew-
               etas);
        end
        J(iV) = W*ns0*vt*exp(etas)*( 1-
           rs - (1-rd)*exp(-Vd/kT) );
        Vout = VV;
    end
end
```